

Single reference atomic based MW interferometry using EIT

Dangka Shylla and Kanhaiya Pandey¹

¹*Department of Physics, Indian Institute of Technology Guwahati, Guwahati, Assam 781039, India **

(Dated: December 1, 2021)

Recently atomic based MW electrometry is experimentally demonstrated and interferometry has been proposed. The proposed interferometry bypasses the conventional, electrical circuit based MW interferometry in much superior fashion. However, this scheme requires three different references for characterizing the unknown MW field. In this work we theoretically study a scheme to develop an atomic based MW interferometry having only one referenced MW field. This scheme involves magnetic sublevels in the Rydberg states and hence will be suitable in even isotope of Yb or alkaline earth element where there is no complication due to absence of the hyperfine levels. Further, the wavelengths to excite the Rydberg states, are very close and hence cancels the Doppler shift more effectively which increases the amplitude sensitivity. We characterize this system for the phase and the amplitude of the unknown MW field w.r.t to the known field and compare it to the previously studied systems.

PACS numbers:

I. INTRODUCTION

Atomic based standards and measurements have gained lot of reliability and is already established for time and length due to its accuracy, precision, and reproducibility [1]. Atomic based DC and AC (MW and RF) magnetometry is in use at the device level, due to its impressive sensitivity and spatial resolutions [2–6]. However, there are many physical quantities which are yet to be standardized based on the atom. The Microwave (MW) field is one of them. The characterization of the MW field is very important and has immediate applications in the communication and radar technologies specially in active sensing and synthetic aperture [7]. The MW field is generally characterized by the electrical circuit based MW interferometry whose performance is greatly limited by Nyquist thermal noise and the bandwidth of the circuit [8–10]. Recently there was a great boost towards characterization of the MW based upon the atom [11, 12] utilizing the very high electric polarizability of available closely spaced Rydberg states. However there was no progress towards atomic based MW interferometry i.e. complete characterization. This is because previously studied system was insensitive to the phase of the MW fields. In the effort of atomic based MW interferometry recently a loopy ladder system has been proposed [13] in Rb and is expected to be **two orders** of magnitude more sensitive as compared to the experimentally demonstrated MW electrometry [11, 12]. However, the proposed MW interferometry [13] requires three reference MW fields. In this work, we theoretically study a double loopy ladder-system realized in Yb using the magnetic sublevels to propose single reference MW interferometry. The scheme is based upon the interference between the two sub-system causing transparency

of probe which has phase dependency of unknown MW field w.r.t the reference field. This scheme is more suitable in the even isotope of Yb or alkaline earth elements such as Mg, Ca, Sr, where there is no complication due to absence of the hyperfine levels and it is easy to address the magnetic sublevels. Further, the wavelength of the two lasers to excite the Rydberg state, are very close, which cancels the Doppler shift more effectively in the counter-propagating configuration and amplitude sensitivity increases significantly. We characterize this system for the phase and the amplitude of the unknown MW field w.r.t to the known field and compare it to the previously studied systems.

II. MODEL SYSTEM

For our study we choose a double loopy ladder system in even isotope of Yb as shown in Fig. 1a. This scheme is also valid for even isotope of earth alkaline element such as Sr, Ca and Mg which has similar level structure. The transitions from the ground state, $6s^2 \ ^1S_0$ to the first excited singlet state, $6s6p \ ^1P_1$ and from the first excited singlet state, $6s6p \ ^1P_1$ to the Rydberg state, $6snd \ ^1D_2$ are driven by the probe laser at wavelength 398 nm and control laser at wavelength 395 nm respectively. The other transitions from the Rydberg singlet D state $6snd \ ^1D_2$ to another Rydberg singlet P state, $6s(n-1)p \ ^1P_1$ and from the Rydberg singlet Rydberg D state $6snd \ ^1D_2$ to Rydberg singlet P state, $6snp \ ^1P_1$ are driven by the unknown MW field and the reference MW field respectively. The higher Rydberg states of Yb has been theoretically calculated and measured experimentally [14, 15]. The bandwidth of this interferometry can range from MHz ($n \sim 150$), GHz ($n \sim 100$), few tens of GHz ($n \sim 60$) to THz ($n \sim 10$) [14, 15].

We choose the quantization axis along the control and probe laser polarization direction and hence these two lasers drive the π transition. The polarization of the

*Electronic address: kanhaiyapandey@iitg.ernet.in

unknown and the reference MW field is perpendicular to the quantization axis and are decomposed into σ^+ and σ^- polarization. The relevant transition driven by the optical and MW fields are shown in Fig. 1a.

The AC electric field interacting with the atomic system corresponding to the transition $|i\rangle \rightarrow |j\rangle$ is $E_{ij}e^{i(\omega_{ij}t+\phi_{ij})}$, where E_{ij} is the amplitude at frequency, ω_{ij} and ϕ_{ij} is the phase. $\Omega_{ij} = -d_{ij}E_{ij}e^{i\phi_{ij}}/\hbar$ is the Rabi frequency associated with the electric field that couples the $|i\rangle \rightarrow |j\rangle$ transition having dipole moment matrix element d_{ij} . Therefore, we define Ω_{12} and Ω_{23} to be the Rabi frequencies of the probe and the control laser respectively and Ω_{34}^{unk} , $\Omega_{34'}^{\text{unk}}$, Ω_{45}^{unk} , $\Omega_{4'5'}^{\text{unk}}$, Ω_{56}^{ref} , $\Omega_{5'6'}^{\text{ref}}$, Ω_{36}^{ref} and $\Omega_{3'6'}^{\text{ref}}$ to be the Rabi frequencies of the control MW fields. Note that the subscript here denotes the transition driven by them whereas, the superscript ‘unk’ and ‘ref’ refers to the unknown and the reference MW fields respectively. After incorporating the Clebsch Gordan coefficients for the transitions driven by the MW field and the decomposition of the linearly polarized MW electric fields into σ^+ and σ^- we have the following relations $|\Omega_{45}^{\text{unk}}| = \sqrt{6}|\Omega_{34}^{\text{unk}}| = |\Omega_{4'5'}^{\text{unk}}| = \sqrt{6}|\Omega_{34'}^{\text{unk}}| = \frac{1}{\sqrt{2}}|\Omega_{45}^{\text{unk}}|$, where $|\Omega_{45}^{\text{unk}}|$ is the magnitude of the maximum Rabi frequency associated with the transition $6\text{snd } ^1D_2 \rightarrow 6\text{snp } ^1P_1$ transition. Similarly, for the reference MW field we have $|\Omega_{56}^{\text{ref}}| = \sqrt{6}|\Omega_{36}^{\text{ref}}| = |\Omega_{5'6'}^{\text{ref}}| = \sqrt{6}|\Omega_{3'6'}^{\text{ref}}| = \frac{1}{\sqrt{2}}|\Omega_{56}^{\text{ref}}|$.

The schematic representation for the experimental setup of phase dependent MW interferometry is as shown in Fig.1(c) in which a probe laser at 398 nm and a control laser at 395 nm are counter-propagating inside the Yb atomic beam. It is hard to make a glass cell for the alkaline earth element or Yb in this case, as the sublimation temperature of these elements is around 700 K. Hence, the atomic beam is a good option and has already been used previously[16–18]. The typical divergence of a roughly collimated atomic beam corresponds to a transverse temperature of around 1 K. We will be dealing with calculations for 1 K and also in the extreme case of temperature at 700 K where there is no collimation of the atomic beam.

The total Hamiltonian for this system in the dipole moment approximation can be written as

$$\begin{aligned}
H = & \left[\sum_{i=1}^5 \frac{\hbar\Omega_{i,i+1}}{2} (e^{i\omega_{i,i+1}t} + e^{-i\omega_{i,i+1}t}) |i\rangle\langle i+1| \right. \\
& + \sum_{j=4'}^{5'} \frac{\hbar\Omega_{j,j+1}}{2} (e^{i\omega_{j,j+1}t} + e^{-i\omega_{j,j+1}t}) |j\rangle\langle j+1| \\
& + \frac{\hbar\Omega_{36}}{2} (e^{i\omega_{36}t} + e^{-i\omega_{36}t}) |3\rangle\langle 6| \\
& + \frac{\hbar\Omega_{36'}}{2} (e^{i\omega_{36'}t} + e^{-i\omega_{36'}t}) |3\rangle\langle 6'| + h.c. \left. \right] \\
& + \sum_{i=1}^6 \hbar\omega_i |i\rangle\langle i| + \sum_{j=4'}^{6'} \hbar\omega_j |j\rangle\langle j| \quad (1)
\end{aligned}$$

where, $\hbar\omega_i$ and $\hbar\omega_j$ are energies of the states $|i\rangle$ and $|j\rangle$

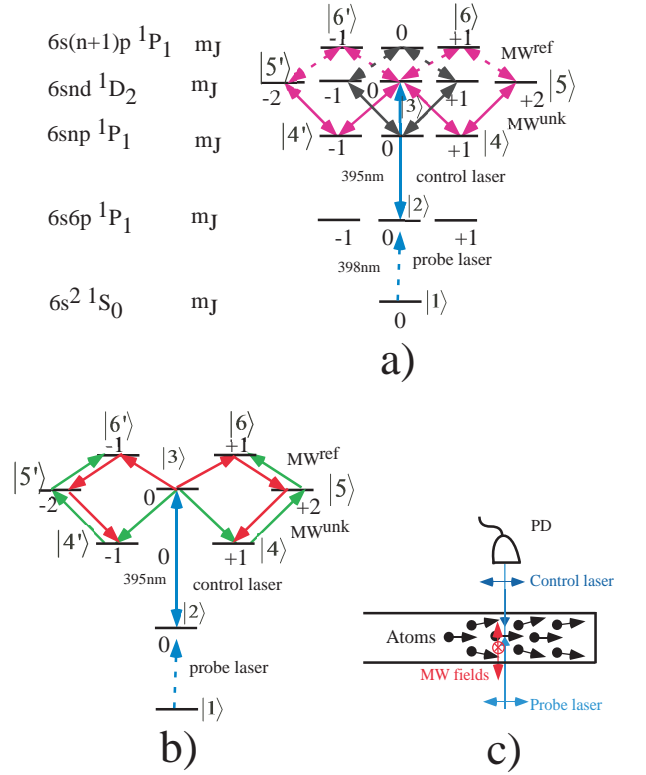


Figure 1: (Color online). (a) The energy level diagram for double loop ladder system for single reference MW interferometry in Yb. (b) Transitions shown by green and red arrow lines are the two sets of sub-systems closing the loop. (c) Schematic representation of the experimental set up to realize the double loop ladder system. It consists of the atomic source, laser beams and MW fields.

respectively.

In the rotating frame with rotating wave approximation the above Hamiltonian can be written as

$$\begin{aligned}
H = & \hbar[0|1\rangle\langle 1| - \delta_{12}|2\rangle\langle 2| - (\delta_{12} + \delta_{23})|3\rangle\langle 3| \\
& - (\delta_{12} + \delta_{23} - \delta_{34})|4\rangle\langle 4| - (\delta_{12} + \delta_{23} - \delta_{34'})|4'\rangle\langle 4'| \\
& - (\delta_{12} + \delta_{23} - \delta_{34} + \delta_{45})|5\rangle\langle 5| - (\delta_{12} + \delta_{23} - \delta_{34'} + \delta_{4'5'})|5'\rangle\langle 5'| \\
& - (\delta_{12} + \delta_{23} - \delta_{34} + \delta_{45} + \delta_{56})|6\rangle\langle 6| \\
& - (\delta_{12} + \delta_{23} - \delta_{34'} + \delta_{4'5'} + \delta_{5'6'})|6'\rangle\langle 6'| \\
& + \frac{\Omega_{12}}{2}|1\rangle\langle 2| + \frac{\Omega_{23}}{2}|2\rangle\langle 3| + \frac{\Omega_{34}}{2}|3\rangle\langle 4| + \frac{\Omega_{34'}}{2}|3\rangle\langle 4'| \\
& + \frac{\Omega_{45}}{2}|4\rangle\langle 5| + \frac{\Omega_{45}}{2}|4'\rangle\langle 5'| + \frac{\Omega_{56}}{2}|5\rangle\langle 6| + \frac{\Omega_{5'6'}}{2}|5'\rangle\langle 6'| \\
& + \frac{\Omega_{36}}{2}e^{i(\delta_{34}-\delta_{45}-\delta_{56}+\delta_{36})t}|3\rangle\langle 6| \\
& + \frac{\Omega_{36'}}{2}e^{i(\delta_{34'}-\delta_{4'5'}-\delta_{5'6'}+\delta_{36'})t}|3\rangle\langle 6'| + h.c. \quad (2)
\end{aligned}$$

where, $\delta_{12} = \omega_{12}^L - (\omega_2 - \omega_1)$, $\delta_{23} = \omega_{23}^L - (\omega_3 - \omega_2)$ are the detunings of the probe and control lasers, $\delta_{34} = \omega_{34}^L - (\omega_3 - \omega_4)$, $\delta_{45} = \omega_{45}^L - (\omega_5 - \omega_4)$, $\delta_{56} = \omega_{56} - (\omega_6 - \omega_5)$, $\delta_{36} = \omega_{36} - (\omega_6 - \omega_3)$ $\delta_{34'} = \omega_{34'}^L - (\omega_3 - \omega_{4'})$, $\delta_{4'5'} =$

$\omega_{4'5'}^L - (\omega_{5'} - \omega_{4'})$, $\delta_{5'6'} = \omega_{5'6'} - (\omega_{6'} - \omega_{5'})$ and $\delta_{36'} = \omega_{36} - (\omega_{6'} - \omega_3)$ are the detunings for the MW fields for the respective transitions. Note that the Hamiltonian H is time dependent except for a particular condition when $\delta_{34} - \delta_{45} - \delta_{56} + \delta_{36} = 0$ and $\delta_{34'} - \delta_{4'5'} - \delta_{5'6'} + \delta_{36'} = 0$. To investigate the dynamics of the double loopy ladder atomic system, we employ the density matrix approach using Liouville's equation. This equation gives the time evolution of the density matrix, ρ as $\dot{\rho} = \frac{i}{\hbar}[H, \rho] - \frac{1}{2}\{\Gamma, \rho\}$ where, Γ is the relaxation matrix. The advantage of using this equation is the fact that it contains both statistical as well as quantum mechanical information about the system which on solving, yields the following set of differential equations:

$$\begin{aligned}
\dot{\rho}_{12} &= i\frac{\Omega_{12}}{2}(\rho_{11} - \rho_{22}) + i\frac{\Omega_{23}^*}{2}\rho_{13} - \gamma_{12}\rho_{12} \\
\dot{\rho}_{13} &= -\gamma_{13}\rho_{13} - i\frac{\Omega_{12}}{2}\rho_{23} + i\frac{\Omega_{23}}{2}\rho_{12} + i\frac{\Omega_{34}^*}{2}\rho_{14} \\
&\quad + i\frac{\Omega_{34'}^*}{2}\rho_{14'} + i\frac{\Omega_{36}^*}{2}e^{-i(\delta_{34} - \delta_{45} - \delta_{56} + \delta_{36})t}\rho_{16} \\
&\quad + i\frac{\Omega_{36}^*}{2}e^{-i(\delta_{34'} - \delta_{4'5'} - \delta_{5'6'} + \delta_{36'})t}\rho_{16'} \\
\dot{\rho}_{14} &= -\gamma_{14}\rho_{14} - i\frac{\Omega_{12}}{2}\rho_{24} + i\frac{\Omega_{34}^{\text{ref}}}{2}\rho_{13} + i\frac{\Omega_{45}^{\text{ref}*}}{2}\rho_{15} \\
\dot{\rho}_{14'} &= -\gamma_{14'}\rho_{14'} - i\frac{\Omega_{12}}{2}\rho_{24'} + i\frac{\Omega_{34'}}{2}\rho_{13} + i\frac{\Omega_{4'5'}^*}{2}\rho_{15'} \\
\dot{\rho}_{15} &= -\gamma_{15}\rho_{15} - i\frac{\Omega_{12}}{2}\rho_{25} + i\frac{\Omega_{45}}{2}\rho_{14} + i\frac{\Omega_{56}^*}{2}\rho_{16} \\
\dot{\rho}_{15'} &= -\gamma_{15'}\rho_{15'} - i\frac{\Omega_{12}}{2}\rho_{25'} + i\frac{\Omega_{4'5'}}{2}\rho_{14'} + i\frac{\Omega_{5'6'}^*}{2}\rho_{16'} \\
\dot{\rho}_{16} &= -\gamma_{16}\rho_{16} - i\frac{\Omega_{12}}{2}\rho_{26} + i\frac{\Omega_{36}}{2}e^{i(\delta_{34} - \delta_{45} - \delta_{56} + \delta_{36})t}\rho_{13} \\
&\quad + i\frac{\Omega_{56}}{2}\rho_{15} \\
\dot{\rho}_{16'} &= -\gamma_{16'}\rho_{16'} - i\frac{\Omega_{12}}{2}\rho_{26'} \\
&\quad + i\frac{\Omega_{36'}}{2}e^{i(\delta_{34'} - \delta_{4'5'} - \delta_{5'6'} + \delta_{36'})t}\rho_{13} + i\frac{\Omega_{5'6'}}{2}\rho_{15'} \quad (3)
\end{aligned}$$

Where,

$$\begin{aligned}
\gamma_{12} &= [\gamma_{12}^{\text{dec}} - i\delta_{12}], \\
\gamma_{13} &= [\gamma_{13}^{\text{dec}} - i(\delta_{12} + \delta_{23})], \\
\gamma_{14} &= [\gamma_{14}^{\text{dec}} - i(\delta_{12} + \delta_{23} - \delta_{34})], \\
\gamma_{14'} &= [\gamma_{14'}^{\text{dec}} - i(\delta_{12} + \delta_{23} - \delta_{34'})], \\
\gamma_{15} &= [\gamma_{15}^{\text{dec}} - i(\delta_{12} + \delta_{23} - \delta_{34} + \delta_{45})], \\
\gamma_{15'} &= [\gamma_{15'}^{\text{dec}} - i(\delta_{12} + \delta_{23} - \delta_{34'} + \delta_{4'5'})], \\
\gamma_{16} &= [\gamma_{16}^{\text{dec}} - i(\delta_{12} + \delta_{23} - \delta_{34} + \delta_{45} + \delta_{56})] \text{ and} \\
\gamma_{16'} &= [\gamma_{16'}^{\text{dec}} - i(\delta_{12} + \delta_{23} - \delta_{34'} + \delta_{4'5'} + \delta_{5'6'})]. \\
\gamma_{ij}^{\text{dec}} &= \left(\frac{\Gamma_i + \Gamma_j}{2}\right) \text{ is decoherence rate between level } |i\rangle \text{ and } |j\rangle, \Gamma_i \text{ and } \Gamma_j \text{ is the total decay rates of states } |i\rangle \text{ and } |j\rangle.
\end{aligned}$$

For our calculations, we take the value of γ_{12}^{dec} which is the decoherence rate between level $|1\rangle$ and $|2\rangle$ to be $2\pi \times 14$ MHz. γ_{12}^{dec} is mainly dominated by the natural ra-

diative decay of excited state $6s6p \ ^1P_1, \Gamma_2$ which is found to be $2\pi \times 28$ MHz. We also take $\gamma_{13}^{\text{dec}} = \gamma_{14}^{\text{dec}} = \gamma_{14'}^{\text{dec}} = \gamma_{15}^{\text{dec}} = \gamma_{15'}^{\text{dec}} = \gamma_{16}^{\text{dec}} = \gamma_{16'}^{\text{dec}} = \gamma^{\text{dec}} = 2\pi \times 100$ kHz and these decoherences are mainly dominated by the laser linewidths of the probe and control lasers wavelength as compared to the radiative decay rate which is $2\pi \times 1$ kHz of the Rydberg states[19].

The above equations can be solved by using the weak probe approximation under the steady state condition i.e. $\dot{\rho}_{ij} = 0$ for all i and j . In the case of weak probe approximation, there will be no population transfer and hence the time evolution of the population terms i.e. the diagonal terms of the density matrix can be approximated as $\rho_{11} \approx 1$, $\rho_{22} \approx \rho_{33} \approx \rho_{44} \approx \rho_{55} \approx \rho_{66} \approx \rho_{4'4'} \approx \rho_{5'5'} \approx \rho_{6'6'} \approx 0$. The off-diagonal terms as $\rho_{ij} = \rho_{ji} \approx 0$ for $i = 2, j = 3, 4, 4', 5, 5', 6, 6'$; $i = 3, j = 4, 4', 5, 5', 6, 6'$; $i = 4, j = 5, 5', 6, 6'$ and $i = 5, j = 6, 6'$. After insertion of the approximations in steady state for the above set of differential equations from the density matrix, we obtain the following new set of linear algebraic equations:

$$\begin{aligned}
\rho_{12} &= \frac{i}{2} \frac{\Omega_{12}}{\gamma_{12}} + \frac{i}{2} \frac{\Omega_{23}^*}{\gamma_{12}} \rho_{13} \\
\rho_{13} &= \frac{i}{2} \frac{\Omega_{23}}{\gamma_{13}} \rho_{12} + \frac{i}{2} \frac{\Omega_{34}^*}{\gamma_{13}} \rho_{14} + \frac{i}{2} \frac{\Omega_{34'}^*}{\gamma_{13}} \rho_{14'} + \frac{i}{2} \frac{\Omega_{36}^*}{\gamma_{13}} \rho_{16} \\
&\quad + \frac{i}{2} \frac{\Omega_{36}^*}{\gamma_{13}} \rho_{16'} \\
\rho_{14} &= \frac{i}{2} \frac{\Omega_{34}}{\gamma_{14}} \rho_{13} + \frac{i}{2} \frac{\Omega_{45}^*}{\gamma_{14}} \rho_{15} \\
\rho_{14'} &= \frac{i}{2} \frac{\Omega_{34'}}{\gamma_{14'}} \rho_{13} + \frac{i}{2} \frac{\Omega_{4'5'}^*}{\gamma_{14'}} \rho_{15'} \\
\rho_{15} &= \frac{i}{2} \frac{\Omega_{45}}{\gamma_{15}} \rho_{14} + \frac{i}{2} \frac{\Omega_{56}^*}{\gamma_{15}} \rho_{16} \\
\rho_{15'} &= \frac{i}{2} \frac{\Omega_{4'5'}}{\gamma_{15'}} \rho_{14'} + \frac{i}{2} \frac{\Omega_{5'6'}^*}{\gamma_{15'}} \rho_{16'} \\
\rho_{16} &= \frac{i}{2} \frac{\Omega_{36}}{\gamma_{16}} \rho_{13} + \frac{i}{2} \frac{\Omega_{56}}{\gamma_{16}} \rho_{15} \\
\rho_{16'} &= \frac{i}{2} \frac{\Omega_{36'}}{\gamma_{16'}} \rho_{13} + \frac{i}{2} \frac{\Omega_{5'6'}}{\gamma_{16'}} \rho_{15'} \quad (4)
\end{aligned}$$

The density matrix element, ρ_{12} is potentially related to the refractive index n of the probe laser as $n = 1 + 3\lambda_p^2 N / (2\pi)(\Gamma_2 / \Omega_{12}) \rho_{12}$ in which $\lambda_p = 398$ nm is the wavelength of the probe laser and N is atomic number density[20, 21]. In order to establish an analytical formulation for ρ_{12} which is directly proportional to the absorption experienced by the probe field, we solve the above linear algebraic equations. The above equations gives solution for ρ_{12} as

$$\rho_{12} = \frac{\frac{i}{2} \frac{\Omega_{12}}{\gamma_{12}}}{1 + \frac{\frac{|\Omega_{23}|^2}{4 \gamma_{12} \gamma_{13}}}{1 + \frac{|\Omega_{34}^{\text{unk}}|^2}{4 \gamma_{13} \gamma_{14}} + \frac{|\Omega_{45}^{\text{unk}}|^2}{4 \gamma_{14} \gamma_{15}} + \text{Int} + \frac{|\Omega_{36}^{\text{ref}}|^2}{4 \gamma_{13} \gamma_{16}} + \frac{|\Omega_{56}^{\text{ref}}|^2}{4 \gamma_{15} \gamma_{16}} + \text{Int}'}}$$
(5)

Where,

$$\text{EITATA1} = \frac{\frac{1}{4} \frac{|\Omega_{34}^{\text{unk}}|^2}{\gamma_{13} \gamma_{14}}}{1 + \frac{\frac{1}{4} \frac{|\Omega_{45}^{\text{unk}}|^2}{\gamma_{14} \gamma_{15}}}{1 + \frac{1}{4} \frac{|\Omega_{56}^{\text{ref}}|^2}{\gamma_{15} \gamma_{16}}}}; \text{EITATA2} = \frac{\frac{1}{4} \frac{|\Omega_{36}^{\text{ref}}|^2}{\gamma_{13} \gamma_{16}}}{1 + \frac{\frac{1}{4} \frac{|\Omega_{45}^{\text{unk}}|^2}{\gamma_{14} \gamma_{15}}}{1 + \frac{1}{4} \frac{|\Omega_{56}^{\text{ref}}|^2}{\gamma_{15} \gamma_{16}}}}$$
(6)

$$\text{EITATA1}' = \frac{\frac{1}{4} \frac{|\Omega_{34'}^{\text{unk}}|^2}{\gamma_{13} \gamma_{14'}}}{1 + \frac{\frac{1}{4} \frac{|\Omega_{45'}^{\text{unk}}|^2}{\gamma_{14'} \gamma_{15'}}}{1 + \frac{1}{4} \frac{|\Omega_{56'}^{\text{ref}}|^2}{\gamma_{15'} \gamma_{16'}}}}; \text{EITATA2}' = \frac{\frac{1}{4} \frac{|\Omega_{36'}^{\text{ref}}|^2}{\gamma_{13} \gamma_{16'}}}{1 + \frac{\frac{1}{4} \frac{|\Omega_{45'}^{\text{unk}}|^2}{\gamma_{14'} \gamma_{15'}}}{1 + \frac{1}{4} \frac{|\Omega_{56'}^{\text{ref}}|^2}{\gamma_{15'} \gamma_{16'}}}}$$
(7)

$$\text{Int} = -\frac{\frac{1}{8} \frac{|\Omega_{34}^{\text{unk}}| |\Omega_{45}^{\text{unk}}| |\Omega_{56}^{\text{ref}}| |\Omega_{36}^{\text{ref}}| \cos(\phi)}{\gamma_{13} \gamma_{14} \gamma_{15} \gamma_{16}}}{1 + \frac{1}{4} \frac{|\Omega_{45}^{\text{unk}}|^2}{\gamma_{14} \gamma_{15}} + \frac{1}{4} \frac{|\Omega_{56}^{\text{ref}}|^2}{\gamma_{15} \gamma_{16}}};$$
(8)

$$\text{Int}' = -\frac{\frac{1}{8} \frac{|\Omega_{34'}^{\text{unk}}| |\Omega_{45'}^{\text{unk}}| |\Omega_{56'}^{\text{ref}}| |\Omega_{36'}^{\text{ref}}| \cos(\phi)}{\gamma_{13} \gamma_{14'} \gamma_{15'} \gamma_{16'}}}{1 + \frac{1}{4} \frac{|\Omega_{45'}^{\text{unk}}|^2}{\gamma_{14'} \gamma_{15'}} + \frac{1}{4} \frac{|\Omega_{56'}^{\text{ref}}|^2}{\gamma_{15'} \gamma_{16'}}};$$
(9)

where, $\phi = \phi_{36}^{\text{ref}} - \phi_{34}^{\text{unk}} - \phi_{45}^{\text{unk}} - \phi_{56}^{\text{ref}} = \phi_{36'}^{\text{ref}} - \phi_{34'}^{\text{unk}} - \phi_{45'}^{\text{unk}} - \phi_{56'}^{\text{ref}} = 2(\phi^{\text{ref}} - \phi^{\text{unk}})$. In order to verify the approximation made above, we have checked the analytical solution of ρ_{12} given by the Eq. [5] and the complete numerical solution in the steady state for various values of control fields and detunings. It has excellent agreement between complete numerical and approximated analytical solution.

III. RESULTS AND DISCUSSIONS

In this section, we analyze the probe absorption in presence of the control laser and the MW fields. As shown in Fig. 1a, the unknown and the reference MW field forms three closed loops, out of which two loops $|3\rangle \leftrightarrow |4\rangle \leftrightarrow |5\rangle \leftrightarrow |6\rangle \leftrightarrow |3\rangle$ and $|3\rangle \leftrightarrow |4'\rangle \leftrightarrow |5'\rangle \leftrightarrow |6'\rangle \leftrightarrow |3\rangle$, represented with magenta color are connected to the control laser and hence contribute to the phase sensitive modification of the absorption of the probe laser. The loop represented with black color is not connected with control laser and hence it is idle for the probe absorption. The first closed loop, $|3\rangle \leftrightarrow |4\rangle \leftrightarrow |5\rangle \leftrightarrow |6\rangle \leftrightarrow |3\rangle$ can be realized by two sub-systems $|3\rangle \rightarrow |4\rangle \rightarrow |5\rangle \rightarrow |6\rangle$ and $|3\rangle \rightarrow |6\rangle \rightarrow |5\rangle \rightarrow |4\rangle$ shown with red and green arrows respectively sharing a common $|1\rangle \rightarrow |2\rangle \rightarrow |3\rangle$ ladder system. Similarly, the second loop $|3\rangle \leftrightarrow |4'\rangle \leftrightarrow |5'\rangle \leftrightarrow |6'\rangle \leftrightarrow |3\rangle$ can be also realized by two sub-systems $|3\rangle \rightarrow |4'\rangle \rightarrow |5'\rangle \rightarrow |6'\rangle$ and $|3\rangle \rightarrow |6'\rangle \rightarrow |5'\rangle \rightarrow |4'\rangle$ shown with red and green arrows respectively and sharing the same $|1\rangle \rightarrow |2\rangle \rightarrow |3\rangle$ ladder system as shown in Fig. 1b.

To realize the functions of various control fields, we activate them one by one in the following sequence. But let us consider only the first loop and the second loop later on as it is evident that the same process occurs in the second loop. The control laser, Ω_{23} causes reduction in the absorption of the probe laser, Ω_{12} and is known as EIT. For the path shown with the green arrows, the control field, Ω_{34}^{unk} recovers the absorption against the EIT and is known as EITA [22]. In a similar way, the control fields Ω_{45}^{unk} and Ω_{56}^{ref} causes EITAT and EITATA [22] expressed by **EITATA1** in Eq. [5]. The other path shown with red arrows will also cause EITATA but by sequence of the control fields Ω_{36}^{ref} , Ω_{56}^{ref} , Ω_{45}^{unk} and Ω_{34}^{unk} , which is expressed by **EITATA2** in Eq. [5]. The term int in the expression of ρ_{12} corresponds to the interference between the two sub-systems causing **EITATA1** and **EITATA2** and is phase ϕ dependent. Similarly, in the second loop the path shown with green arrows by sequence of control fields $\Omega_{34'}$, $\Omega_{45'}$, $\Omega_{56'}^{\text{ref}}$ and $\Omega_{36'}$ causes **EITATA1'** in Eq. [5]. Also, in other path shown with red arrows will cause **EITATA2'** by sequence of the control fields $\Omega_{36'}^{\text{ref}}$, $\Omega_{56'}^{\text{ref}}$, $\Omega_{45'}$ and $\Omega_{34'}$ in Eq. [5]. Likewise, the term int' in the expression of ρ_{12} corresponds to the interference between the two sub-systems causing **EITATA1'** and **EITATA2'** and is phase ϕ dependent as well.

We define the normalized absorption $[(\Gamma_2/\Omega_{12})\text{Im}(\rho_{12})]$ i.e. for the stationary atoms the absorption of the probe laser at resonance in the absence of all the control lasers is 1 as shown by the peak of the black curve in Fig.2. First, we investigate the normalized absorption $(\text{Im}(\rho_{12})\Gamma_2/\Omega_{12})$ vs probe detuning (δ_{12}) for three different phases, $\phi = 0, \pi/2$ and π as shown in Fig. 2. The double loopy ladder systems $|1\rangle \rightarrow |2\rangle \leftrightarrow |3\rangle \leftrightarrow |4\rangle \leftrightarrow |5\rangle \leftrightarrow |6\rangle$ and $|1\rangle \rightarrow |2\rangle \leftrightarrow |3\rangle \leftrightarrow |4'\rangle \leftrightarrow |5'\rangle \leftrightarrow |6'\rangle$ are symmetric with overlapping absorption peaks for $\delta_{14} = \delta_{14'}$, $\delta_{15} = \delta_{15'}$, $\delta_{16} = \delta_{16'}$, $\Omega_{34}^{\text{unk}} = \Omega_{34'}^{\text{unk}}$, $\Omega_{45}^{\text{unk}} = \Omega_{45'}^{\text{unk}}$, $\Omega_{36}^{\text{ref}} = \Omega_{36'}^{\text{ref}}$ and $\Omega_{56}^{\text{ref}} = \Omega_{56'}^{\text{ref}}$. For $\phi = 0$ at line center of the probe absorption, the two sets of sub system causing **EITATA1** and **EITATA2** or **EITATA1'** and **EITATA2'** interfere destructively with each other and there is transparency. But for $\phi = \pi$, the two sets of sub systems causing **EITATA1** and **EITATA2** or **EITATA1'** and **EITATA2'** interfere constructively with each other and there is maximum absorption.

For large Rabi frequencies of the control laser and MW fields, the absorption peaks are well separated. This separation, the linewidth and the amplitude of these can be well understood using the dressed state approach. For general control fields detunings and Rabi frequencies, the position of the absorption peaks (dressed states) will be complicated. However, the expression becomes straightforward at zero detunings of the control field and the MW fields. The central dressed state is a superposition of the bare atomic states and is expressed as $\frac{1}{\sqrt{A}} \left[\frac{-e^{i\phi} |\Omega_{36}^{\text{ref}}| |\Omega_{45}^{\text{unk}}| + |\Omega_{34}^{\text{unk}}| |\Omega_{56}^{\text{ref}}|}{|\Omega_{23}| |\Omega_{45}^{\text{unk}}|} |2\rangle - \frac{|\Omega_{56}^{\text{ref}}|}{|\Omega_{45}^{\text{unk}}|} (|4\rangle + |6\rangle) \right]$, where $A = \left[\frac{-e^{i\phi} |\Omega_{36}^{\text{ref}}| |\Omega_{45}^{\text{unk}}| + |\Omega_{34}^{\text{unk}}| |\Omega_{56}^{\text{ref}}|}{|\Omega_{23}| |\Omega_{45}^{\text{unk}}|} \right]^2 + \frac{|\Omega_{56}^{\text{ref}}|^2}{|\Omega_{45}^{\text{unk}}|^2} + 1$. Its linewidth is

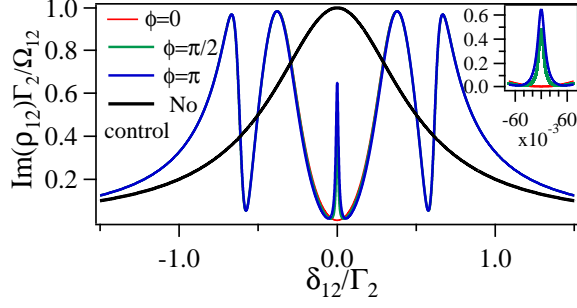


Figure 2: (Color online). Normalized absorption ($\text{Im}(\rho_{12})\Gamma_2/\Omega_{12}$) vs δ_{12}/Γ_2 of the probe laser with $\delta_{23} = \delta_{34} = \delta_{34'} = \delta_{45} = \delta_{4'5'} = \delta_{56} = \delta_{5'6'} = \delta_{36} = \delta_{36'} = 0$, $|\Omega_{23}| = \Gamma_2$, $|\Omega^{\text{ref}}| = \sqrt{2}\Gamma_2$ and $|\Omega^{\text{unk}}| = \sqrt{2} \times 0.1\Gamma_2$. The inset is a zoomed absorption profile around the central peak.

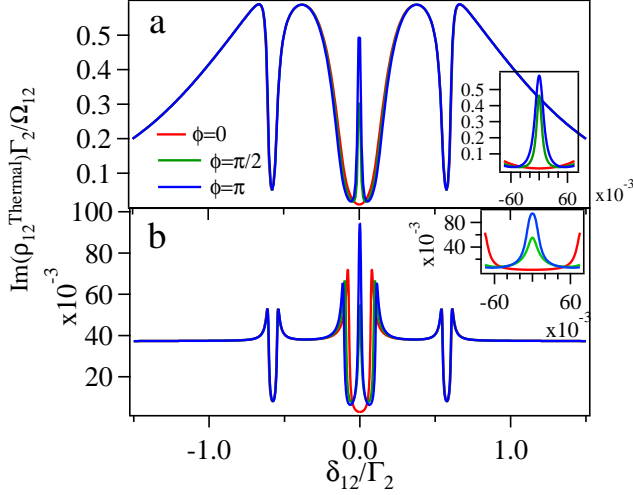


Figure 3: (Color online). Normalized absorption of the probe laser with thermal averaging ($\text{Im}(\rho_{12}^{\text{Thermal}})\Gamma_2/\Omega_{12}$) vs δ_{12}/Γ_2 of the probe laser with $\delta_{23} = \delta_{34} = \delta_{34'} = \delta_{45} = \delta_{4'5'} = \delta_{56} = \delta_{5'6'} = \delta_{36} = \delta_{36'} = 0$, $|\Omega_{23}| = \Gamma_2$, $|\Omega^{\text{ref}}| = \sqrt{2}\Gamma_2$ and $|\Omega^{\text{unk}}| = \sqrt{2} \times 0.1\Gamma_2$. (a) $T=1$ K (b) $T=700$ K. The insets are zoomed absorption profile around the central peak of (a) and (b).

given by $\frac{1}{A} \left[\frac{-e^{i\phi} |\Omega_{36}^{\text{ref}}| |\Omega_{45}^{\text{unk}}| + |\Omega_{34}^{\text{unk}}| |\Omega_{56}^{\text{ref}}|}{|\Omega_{23}| |\Omega_{45}^{\text{unk}}|} \right]^2 \Gamma_2 + \frac{|\Omega_{36}^{\text{ref}}|^2}{|\Omega_{45}^{\text{unk}}|^2} \Gamma_4 + \Gamma_6$ which depends on the phase. The amplitude of the peak is proportional to $\frac{1}{A} \left| \frac{-e^{i\phi} |\Omega_{36}^{\text{ref}}| |\Omega_{45}^{\text{unk}}| + |\Omega_{34}^{\text{unk}}| |\Omega_{56}^{\text{ref}}|}{|\Omega_{23}| |\Omega_{45}^{\text{unk}}|} \right|^2 = \frac{(1 - \cos\phi) \frac{|\Omega_{23}^{\text{ref}}|^2}{3|\Omega_{23}|^2}}{(1 - \cos\phi) \frac{|\Omega_{23}^{\text{ref}}|^2}{3|\Omega_{23}|^2} + \frac{|\Omega_{\text{unk}}^{\text{ref}}|^2}{|\Omega_{\text{unk}}|^2} + 1}$.

From this expression it is clear that the probe absorption is zero at $\phi = 0$ and is maximum at $\phi = \pi$.

Now, we investigate the effect of temperature on the absorption profile considering the atomic beam to be divergent. The thermal averaging of ρ_{12} is done numeri-

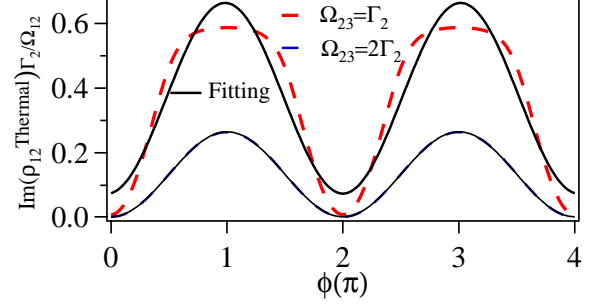


Figure 4: (Color online). Absorption of the probe laser after thermal averaging ($\text{Im}(\rho_{12}^{\text{Thermal}})\Gamma_2/\Omega_{12}$) vs $\phi(\pi)$ at $T=1$ K, with $\delta_{12} = \delta_{23} = \delta_{34} = \delta_{34'} = \delta_{45} = \delta_{4'5'} = \delta_{56} = \delta_{5'6'} = \delta_{36} = \delta_{36'} = 0$, $|\Omega^{\text{ref}}| = \sqrt{2}\Gamma_2$ and $|\Omega^{\text{unk}}| = \sqrt{2} \times 0.1\Gamma_2$.

cally at two temperatures i.e. at $T=1$ K and at $T=700$ K for the counter-propagating configuration of the probe (Ω_{12}) and the control lasers (Ω_{23}) with wave vectors k_{398} and k_{395} respectively, by replacing δ_{12} with $\delta_{12} + k_{398}v$ and δ_{23} with $\delta_{23} - k_{395}v$ for moving atoms with velocity v , while the Doppler shift for the MW fields are ignored. Further, the ρ_{12} is weighted by the Maxwell Boltzman velocity distribution function and integrated over the velocity as $\rho_{12}^{\text{Thermal}} = \sqrt{\frac{m}{2\pi k_B T}} \int \rho_{12}(v) e^{-\frac{mv^2}{2k_B T}} dv$, where k_B is Boltzman constant and m is the atomic mass of Yb. The integration is done over velocity range which is two times of $\sqrt{\frac{k_B T}{m}}$. Unlike the previously studied system in Rb [13] the two-photon Doppler mismatch for the probe and the control lasers here is very small in comparison to Γ_2 as the wavelength of two optical transition are very close due to which there is no broadening of the central absorption peak as shown in Fig. 3 by thermal averaging. The narrowing of the EIT window and the enhanced absorption at the wing is still observed which has been extensively studied previously [23–26].

Next, we study the probe absorption after thermal averaging vs the phase ϕ with all the detunings at zero. From the plot shown with the red dashed line in Fig. 4, we observe more than 95% change in the probe absorption for the change of phase from 0 to π for $|\Omega^{\text{unk}}| = \sqrt{2} \times 0.1\Gamma_2$ and for the input parameters i.e. $\Omega_{23} = \Gamma_2$ and $|\Omega^{\text{ref}}| = \sqrt{2}\Gamma_2$. The numerical data shown by dotted red curve is fitted by a function $A+B\sin(f\phi+\theta)$, where A , B , f and θ are kept as free parameters, the fitting is shown with a black curve in Fig. 4. This shows a strong deviation from the sinusoidal behavior. In order to have sinusoidal behavior we increase the Ω_{23} to $2\Gamma_2$ as shown with dotted blue trace.

To measure the phase and amplitude/strength of the unknown MW field, we define a quantity, $S = \text{Im}[\rho_{12}^{\text{Thermal}}(\phi = 0) - \rho_{12}^{\text{Thermal}}(\phi = \pi)] / \text{Im}[\rho_{12}^{\text{Thermal}}(\phi = 0) + \rho_{12}^{\text{Thermal}}(\phi = \pi)]$. We plot S for different values of $|\Omega^{\text{unk}}|$ as a function of

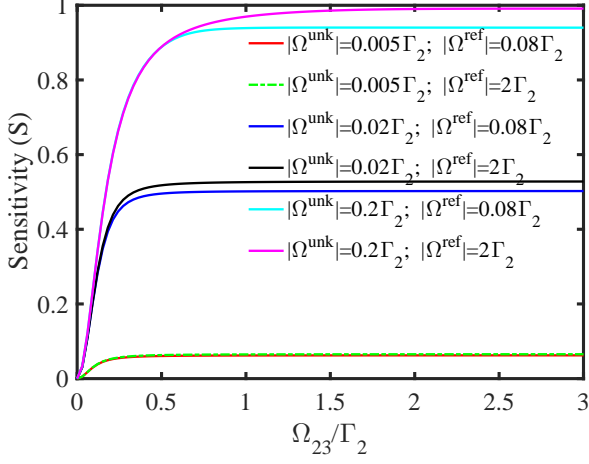


Figure 5: (Color online). S vs Ω_{23}/Γ_2 with $\delta_{12} = \delta_{23} = \delta_{34} = \delta_{34'} = \delta_{45} = \delta_{4'5'} = \delta_{56} = \delta_{5'6'} = \delta_{36} = \delta_{36'} = 0$.

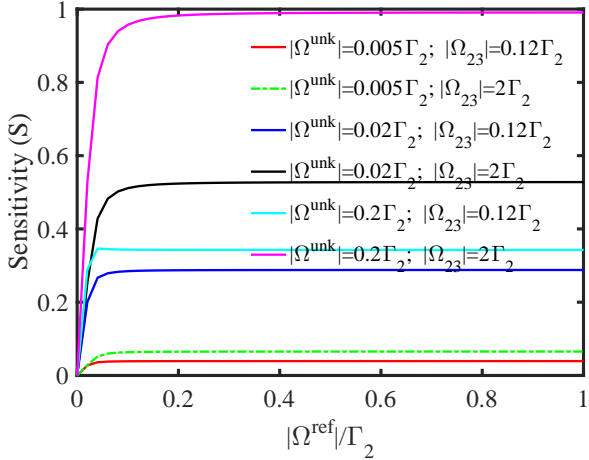


Figure 6: (Color online). S vs $|\Omega^{\text{ref}}|/\Gamma_2$ with $\delta_{12} = \delta_{23} = \delta_{34} = \delta_{34'} = \delta_{45} = \delta_{4'5'} = \delta_{56} = \delta_{5'6'} = \delta_{36} = \delta_{36'} = 0$.

the input parameters, Ω_{23} and $|\Omega^{\text{ref}}|$ in Fig. 5 and Fig. 6 respectively. From the figures it is clear that the sensitivity S increases with Ω_{23} and $|\Omega^{\text{ref}}|$ and then it saturates. The saturation points on Ω_{23} and $|\Omega^{\text{ref}}|$ increase with increment of $|\Omega^{\text{unk}}|$.

We also compare the strength sensitivity for the MW field, between the previously studied four-level [12] and six-level loopy [13] ladder systems in Rb with the system studied in this work i.e. the double loopy ladder system in Yb. The sensitivity for the various systems are plotted in Fig. 7. The sensitivity of the double loopy ladder system in Yb is much higher than the four-level [12] system. This is due to the fact that the effect of small $|\Omega^{\text{unk}}|$ gets amplified by the strong control $|\Omega^{\text{ref}}|$ as both appears in multiplication inside the \mathbf{int} and \mathbf{int}' terms in Eq. 8 and

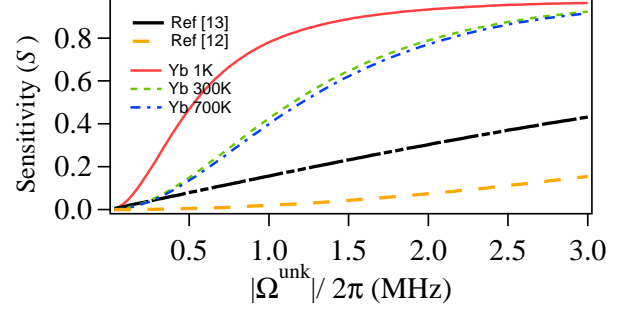


Figure 7: (Color online). (a) S for various system vs $|\Omega^{\text{unk}}|/2\pi(\text{MHz})$ with $\delta_{12} = \delta_{23} = \delta_{34} = \delta_{34'} = \delta_{45} = \delta_{4'5'} = \delta_{56} = \delta_{5'6'} = \delta_{36} = \delta_{36'} = 0$ and optimized Rabi frequencies of control fields in individual case.

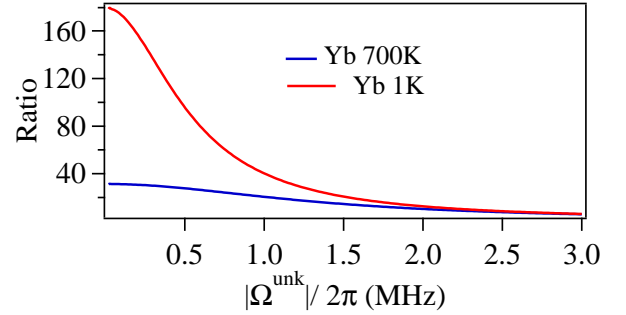


Figure 8: (Color online). Ratio of the sensitivities between the double loopy ladder system and the system in Ref. [12] vs $|\Omega^{\text{unk}}|/2\pi(\text{MHz})$ with $\delta_{12} = \delta_{23} = \delta_{34} = \delta_{34'} = \delta_{45} = \delta_{4'5'} = \delta_{56} = \delta_{5'6'} = \delta_{36} = \delta_{36'} = 0$.

Eq. 9 respectively. The ratio of the sensitivities between the two systems vs $|\Omega^{\text{unk}}|$ at two different temperature is plotted in the Fig. 8.

We also plot the ratio of sensitivities between the double loopy ladder system to the system in Ref. [12] vs sensitivity of double loopy ladder system which gives the information about the possibility of the detection of $|\Omega^{\text{unk}}|$. This is an important plot because there is a possibility that the ratio is large but cannot be detected by the double loopy ladder system in Yb. This detection of the Sensitivity, S upto 1% is very much possible by using locking detection. At this value, the ratio of the sensitivities between the double loopy ladder system in Yb and the four-level system in Rb at 1 K and 700 K [12] will be around 200 and 40 respectively as shown in Fig. 9.

The higher sensitivity of this system with respect to the six-level loopy ladder system[13] in Rb is due to very small mismatch of Doppler shift for the probe at 398 nm and the control laser 395 nm as compared to the probe at 780 nm and the control laser at 480 nm used in Rb[13].

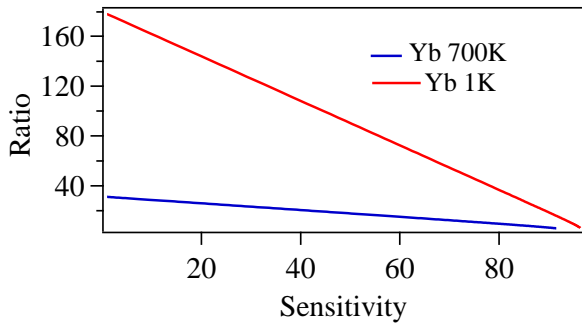


Figure 9: (Color online). Ratio of the sensitivities between the double loop ladder system and the system in Ref. [12] vs sensitivity of the double loop ladder system.

IV. CONCLUSIONS

In conclusion, we theoretically study a scheme to develop the single reference atomic based MW interferometry in Yb using Rydberg states instead of three reference MW fields as compared to our previous study. This is

based upon the interference between the two sets of subsystems causing EITATA. The interference is either constructive or destructive depending upon the phase of the unknown MW field w.r.t reference MW field. Thereby, this system provides a great opportunity to characterize the MW electric fields completely including the propagation direction and the wavefront. Further, this system is **two orders** of magnitude more sensitivity to the field strength as compared to previous experimental demonstration on MW electrometry. The bandwidth of the atomic based interferometry ranges from MHz, GHz upto THz. This work will be quite useful in the areas of communications particularly in active radar technologies and synthetic aperture radar interferometry.

V. ACKNOWLEDGMENT

K.P. would like to acknowledge the funding from SERB of grant No. ECR/2017/000781 and discussion with David Wilkowski at CQT NTU. D.S. would like to acknowledge the financial support from the Council of Scientific and Industrial Research, India.

-
- [1] J. L. Hall, *Rev. Mod. Phys.* **78**, 1279 (2006), URL <http://link.aps.org/doi/10.1103/RevModPhys.78.1279>.
- [2] D. Budker and M. Romalis, *Nat Phys* **3**, 227 (2007), URL <http://dx.doi.org/10.1038/nphys566>.
- [3] M. Loretz, T. Rosskopf, and C. L. Degen, *Phys. Rev. Lett.* **110**, 017602 (2013), URL <http://link.aps.org/doi/10.1103/PhysRevLett.110.017602>.
- [4] A. Horsley, G.-X. Du, M. Pellaton, C. Afolderbach, G. Mileti, and P. Treutlein, *Phys. Rev. A* **88**, 063407 (2013), URL <https://link.aps.org/doi/10.1103/PhysRevA.88.063407>.
- [5] A. Horsley, G.-X. Du, and P. Treutlein, *New Journal of Physics* **17**, 112002 (2015), URL <http://stacks.iop.org/1367-2630/17/i=11/a=112002>.
- [6] C. Herbert, L. L. Yuan, and R. Dumke, *Scientific Reports* **5** (2015/10/20), URL <http://dx.doi.org/10.1038/srep15448>.
- [7] R. Bamler and P. Hartl, *Inverse Problems* **14**, R1 (1998), URL <http://stacks.iop.org/0266-5611/14/i=4/a=001>.
- [8] R. J. King and Y. H. Yen, *IEEE Transactions on Microwave Theory and Techniques* **29**, 1225 (1981), ISSN 0018-9480.
- [9] E. N. Ivanov and M. E. Tobar, *Review of Scientific Instruments* **80**, 044701 (2009), <http://dx.doi.org/10.1063/1.3115206>, URL <http://dx.doi.org/10.1063/1.3115206>.
- [10] E. N. Ivanov, M. E. Tobar, and R. A. Woode, *IEEE Transactions on Ultrasonics, Ferroelectrics, and Frequency Control* **45**, 1526 (1998), ISSN 0885-3010.
- [11] K. H. S. P., BaluksianT, LowR, and PfauT, *Nat Photon* **4**, 112 (2010), URL <http://dx.doi.org/10.1038/nphoton.2009.260>.
- [12] J. A. Sedlacek, A. Schwettmann, H. Kubler, LowR, PfauT, and J. P. Shaffer, *Nat Phys* **8**, 819 (2012), URL <http://dx.doi.org/10.1038/nphys2423>.
- [13] D. Shylla, E. N. Ogaro, and K. Pandey, *Scientific Reports* **8**, 8692 (2018), URL <https://doi.org/10.1038/s41598-018-27011-1>.
- [14] E. P. Vidolova-Angelova, L. N. Ivanov, and V. S. Letokhov, *J. Opt. Soc. Am.* **71**, 699 (1981), URL <http://www.osapublishing.org/abstract.cfm?URI=josa-71-6-699>.
- [15] C. B. Xu, X. Y. Xu, W. Huang, M. Xue, and D. Y. Chen, *Journal of Physics B: Atomic, Molecular and Optical Physics* **27**, 3905 (1994), URL <http://stacks.iop.org/0953-4075/27/i=17/a=014>.
- [16] D. Das, S. Barthwal, A. Banerjee, and V. Nataraajan, *Phys. Rev. A* **72**, 032506 (2005), URL <https://link.aps.org/doi/10.1103/PhysRevA.72.032506>.
- [17] K. Pandey, A. K. Singh, P. V. K. Kumar, M. V. Suryanarayana, and V. Nataraajan, *Phys. Rev. A* **80**, 022518 (2009), URL <https://link.aps.org/doi/10.1103/PhysRevA.80.022518>.
- [18] T. Yang, K. Pandey, M. S. Pramod, F. Leroux, C. C. Kwong, E. Hajiyev, Z. Y. Chia, B. Fang, and D. Wilkowski, *The European Physical Journal D* **69**, 226 (2015), ISSN 1434-6079, URL <https://doi.org/10.1140/epjd/e2015-60288-y>.
- [19] J. A. Sedlacek, A. Schwettmann, H. Kübler, and J. P. Shaffer, *Phys. Rev. Lett.* **111**, 063001 (2013), URL <http://link.aps.org/doi/10.1103/PhysRevLett.111.063001>.
- [20] J. Gea-Banacloche, Y.-q. Li, S.-z. Jin, and M. Xiao, *Phys. Rev. A* **51**, 576 (1995), URL <https://link.aps.org/doi/10.1103/PhysRevA.51.576>.
- [21] C. C. Kwong, T. Yang, M. S. Pramod, K. Pandey, D. Delande, R. Pierrat, and D. Wilkowski,

- Phys. Rev. Lett. **113**, 223601 (2014), URL <https://link.aps.org/doi/10.1103/PhysRevLett.113.223601>. <http://stacks.iop.org/0953-4075/41/225503>.
- [22] K. Pandey, Phys. Rev. A **87**, 043838 (2013), URL <http://link.aps.org/doi/10.1103/PhysRevA.87.043838>.
- [23] A. Krishna, K. Pandey, A. Wasan, and V. Natarajan, EPL (Europhysics Letters) **72**, 221 (2005), URL <http://stacks.iop.org/0295-5075/72/221>.
- [24] K. Pandey, A. Wasan, and V. Natarajan, Journal of Physics B: Atomic, Molecular and Optical Physics **41**, 225503 (8pp) (2008), URL <http://stacks.iop.org/0953-4075/41/225503>.
- [25] S. M. Iftiquar, G. R. Karve, and V. Natarajan, Phys. Rev. A **77**, 063807 (2008), URL <http://link.aps.org/doi/10.1103/PhysRevA.77.063807>.
- [26] K. Pandey, C. C. Kwong, M. S. Pramod, and D. Wilkowski, Phys. Rev. A **93**, 053428 (2016), URL <http://link.aps.org/doi/10.1103/PhysRevA.93.053428>.